

4f crystal field ground state of the strongly correlated topological insulator SmB₆

M. Sundermann,^{1,2} H. Yavaş,³ K. Chen,¹ D.J. Kim,⁴ Z. Fisk,⁴ D. Kasinathan,²
M. W. Haverkort,⁵ P. Thalmeier,² A. Severing,^{1,2} and L. H. Tjeng²

¹*Institute of Physics II, University of Cologne, Zùlpicher Straße 77, 50937 Cologne, Germany*

²*Max Planck Institute for Chemical Physics of Solids, Nöthnitzer Straße 40, 01187 Dresden, Germany*

³*PETRA III, Deutsches Elektronen-Synchrotron (DESY), Notkestraße 85, 22607 Hamburg, Germany*

⁴*Department of Physics and Astronomy, University of California, Irvine, CA 92697, USA*

⁵*Institute for Theoretical Physics, Heidelberg University, Philosophenweg 19, 69120 Heidelberg, Germany*

We investigated the crystal-electric field ground state of the 4f manifold in the strongly correlated topological insulator SmB₆ using core level non-resonant inelastic x-ray scattering (NIXS). The directional dependence of the scattering function that arises from higher multipole transitions establishes unambiguously that the Γ_8 quartet state of the Sm f^5 $J=5/2$ configuration governs the ground-state symmetry and hence the topological properties of SmB₆.

It was recently proposed that the intermediate valent Kondo insulator SmB₆ [1–5] could be a topological insulator [6–11]. Indeed, topologically protected metallic surface states would be an attractive explanation for the low temperature conductance that has been puzzling scientist for decades. The proposal is appealing since in particular rare earth Kondo insulators have the necessary ingredients for strong spin-orbit coupling and electrons of opposite parity, namely the 4f and 5d. The concept of strongly correlated topological insulators is exciting not only because the surface may have massless charge carriers with locked helical spin polarization but also because the surface of such a strongly correlated system may host novel phenomena not present in semiconductor-based topological insulators [12–15]. With the bulk being truly insulating, SmB₆ has experienced a tremendous renewed interest and many experimental techniques like angle-resolved photoelectron spectroscopy (ARPES) [16–24], scanning tunneling spectroscopy [25–29], resistivity and surface conductance measurements [30–37] have been applied to unveil its topological properties. Please see also Ref. [38, 39] and references therein.

In SmB₆, the strong hybridization of the low lying 4f states with conduction band d states gives rise to a hybridization gap of the order of 20 meV [16–21]. The Fermi level lies in this hybridization gap so that the material is an insulator when the hybridization becomes effective at low temperatures. The strong hybridization also leads to a partial occupation of the 4f shell or a mixture of the Sm f^6 (2+) and f^5 (3+) configurations. For the valence at low temperatures, values of 2.5 to 2.7 are given according to different sources in the literature [40–46]. Hence the electronic structure is described by the Hund's rule ground states of the Sm f^6 (2+) and f^5 (3+) configurations with total orbital momenta of $J=0$ and $5/2$, respectively. The $J=5/2$ multiplet is further split into a Γ_7 doublet and Γ_8 quartet due to the cubic crystal-electric field (CEF). Figure 1 shows the ground state and first excited state of the two Sm configurations plus their electron charge density distributions. The charge densities

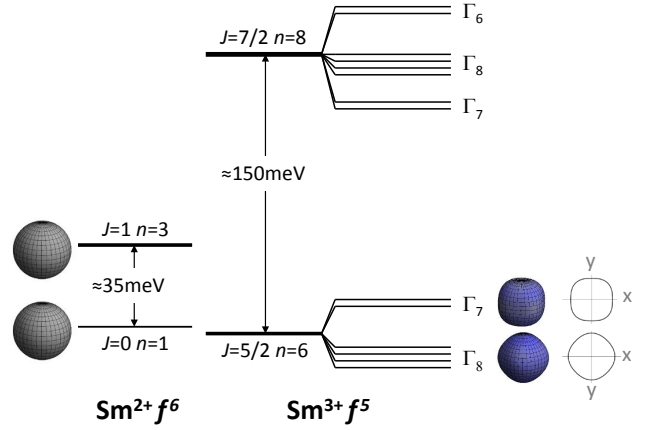


FIG. 1. (color online) Sm²⁺ and Sm³⁺ total energy level diagram. The Sm²⁺ configuration is split into a $J=0$ and $J=1$, and the Sm³⁺ into a $J=5/2$ and $J=7/2$ multiplet. The label n indicates the degeneracy. The Sm³⁺ multiplets are further split (Γ_i) by the cubic crystal-electric field. The insets show the corresponding charge densities for six and five electrons and their 2D projections, respectively.

of the $J=0$ and 1 states are spherical since neither the $J=0$ or 1 are split in a cubic potential [47]. This is contrasted by the charge densities of the CEF split $J=5/2$ multiplet (and $J=7/2$, not shown) that are anisotropic.

Information of the surface topology can be unambiguously inferred from the symmetries and parities of the bulk states involved. Knowledge about the CEF ground state symmetry of SmB₆ therefore plays an essential role. For example, theoretical predictions for the spin texture of the sought-after topological surface states depend very much whether the ground state of the f^5 $J=5/2$ configuration is the Γ_8 quartet or the Γ_7 doublet CEF state. The resulting type or direction of the winding of the spin with wave vector is opposite [48–50].

Surprisingly, after forty years of research, the CEF scheme of SmB₆ has still to be determined. The classical tool inelastic neutron scattering has not been able

to identify the CEF states, possibly due to the superposition of both Sm f^5 and f^6 configurations in this mixed valent compound and the strong neutron absorption despite double isotope samples [51–53]. From inelastic neutron scattering, a sharp excitation at 14 meV close to the hybridization gap was reported. It was assigned to a spin exciton and not to a CEF excitation since its intensity does not follow the $4f$ magnetic form factor. Further magnetic intensities at about 35 meV, 115 meV, and 85 meV have been assigned to the inter-multiplet transitions of the Sm^{2+} configuration and of the CEF split Sm^{3+} configuration (see Fig.1), and to some magnetoelectric coupling, respectively. In-gap transitions at about 15 meV in Raman spectra could be interpreted as CEF excitations but Raman does not yield the information about which state forms the ground state [54, 55]. A semi-empirical extrapolation method can predict CEF parameters across the rare earth series for highly diluted systems [56]. Applying such an extrapolation to the measured CEF schemes of REB_6 with $\text{RE} = \text{Ce}, \text{Pr}$ and Nd [57, 58] yields for SmB_6 a CEF splitting of the order of 15 meV with the Γ_8 quartet as the ground state. However, the Kondo insulator SmB_6 is not a highly diluted system and it is definitely not an ionic system but highly intermediate valent instead, questioning the validity of such an extrapolation.

We, therefore, performed bulk-sensitive, core-level non-resonant inelastic hard-x ray scattering (NIXS) measurements that target specifically the ground state symmetry of SmB_6 . NIXS is a powerful tool to determine the ground state wave function of $4f$ and $5f$ systems [59–62]. This bulk sensitive and element specific spectroscopic method is carried out with large momentum transfers $|\vec{q}|$ so that the transition operator $e^{i\vec{q}\cdot\vec{r}}$ in the scattering function $S(\vec{q},\omega)$ contains contributions of higher multipole terms, giving information that is not accessible in a dipole experiment [63–74]. Here, the dependence of $S(\vec{q},\omega)$ on the direction of vector \vec{q} with respect to the crystallographic lattice provides the symmetry information of the ground state wave function, even for cubic compounds thanks to the multipole terms [67, 75].

The NIXS measurements on the Sm and Eu $N_{4,5}$ core level ($4d^{10}4f^5 \rightarrow 4d^94f^6$ and $4d^{10}4f^6 \rightarrow 4d^94f^7$, respectively) were performed at the beamline P01 of PETRA-III. The incident energy was selected with a Si(311) double monochromator. The P01 NIXS end station has a vertical geometry with twelve Si(660) 1 m radius spherically bent crystal analyzers that are arranged in 3×4 array as shown in Fig. 2 of Ref. 75. The fixed final energy was 9690 eV. The analyzers were positioned at scattering angles of $2\theta \approx 150^\circ, 155^\circ$, and 160° which provide an averaged momentum transfer of $|\vec{q}| = (9.6 \pm 0.1) \text{ \AA}^{-1}$. The scattered beam was detected by a position sensitive custom-made Lambda detector, based on a Medipix3 chip detector. The elastic line was consistently measured and a pixel wise calibration yields an instrumental en-

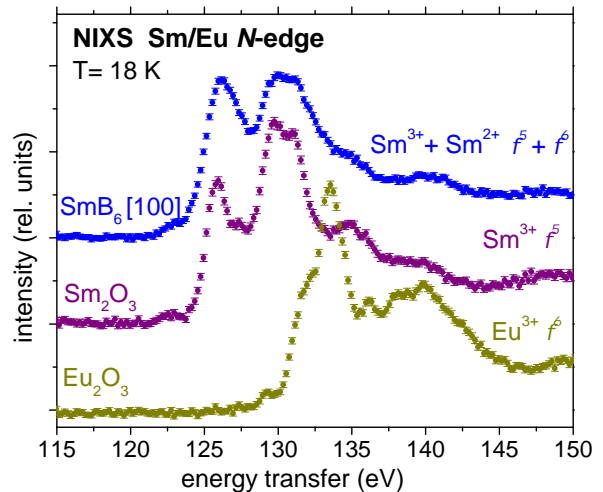


FIG. 2. (color online) Energy scans at the $N_{4,5}$ edges of SmB_6 , Sm_2O_3 and Eu_2O_3 measured with a constant final energy of 9690 eV and 0.2 eV energy steps at $|\vec{q}| = (9.6 \pm 0.1) \text{ \AA}^{-1}$. A linear background has been subtracted.

ergy resolution of ≈ 0.7 eV full width at half maximum (FWHM).

The SmB_6 single crystals used in our study were grown by the aluminum flux method [34]. We have also used commercial polycrystalline Sm_2O_3 and Eu_2O_3 samples (pressed pellets) with 99.9% and 99.99% purity, respectively, as references for a $4f^5$ and $4f^6$ system. Two SmB_6 single crystals with (100) and (110) surfaces were mounted in a vacuum cryostat with Kapton windows. The measurements were performed at 16 K. The two samples were oriented such that for $\vec{q} \parallel [100]$ and $\vec{q} \parallel [110]$ a specular scattering geometry was realized. For the $\vec{q} \parallel [111]$ direction one of the crystals was turned accordingly with respect to the scattering triangle. The reference compounds were measured under the same conditions.

Fig. 2 shows the NIXS spectra across the $N_{4,5}$ edges of SmB_6 (blue dots) and of the two reference compounds Sm_2O_3 and Eu_2O_3 (purple and dark yellow) after subtraction of a linear background and scaling to the Compton background. Spectra over a larger energy interval showing also the elastic lines and the Compton background are given in Fig.S1 of the Appendix. The Eu edge appears at a higher energy transfer than in the case of Sm because Eu has a higher atomic number.

We first investigate whether the SmB_6 spectrum can be interpreted using those of Sm_2O_3 and Eu_2O_3 . For this purpose we construct a spectrum made up of the weighted sum of Sm_2O_3 and Eu_2O_3 . Here the Sm reference is weighted with a factor 0.6 and the one of Eu with a factor of 0.4. In addition, the Eu_2O_3 spectrum is shifted by 6.8 eV to lower energies in order to account for the

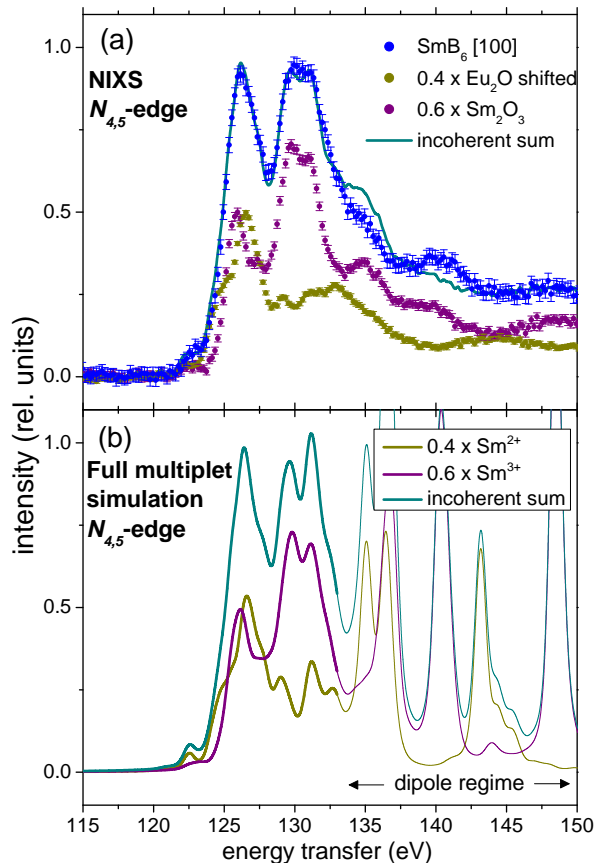


FIG. 3. (color online) (a) Experimental SmB_6 data for $\vec{q}||[100]$ (blue dots) together with the weighted sum (dark cyan line) of the experimental Sm_2O_3 (f^5) (purple dots) and energy shifted experimental Eu_2O_3 (f^6) (dark yellow dots). (b) Full multiplet simulation of Sm^{3+} (purple line) and Sm^{2+} spectra (dark yellow line) and their weighted sum (dark cyan line).

higher atomic number. The resulting spectrum reproduces the SmB_6 spectrum very satisfactorily (see dark cyan line in Fig. 3 (a)). The weights used for the sum corresponds to a Sm valence of 2.6, in good agreement with other studies using a variety of different experimental methods [40–46]. This provides us with confidence to carry out further analysis using full multiplet calculations based on the $4f^5$ and $4f^6$ configurations of Sm.

Fig. 3 (b) shows the full multiplet simulation of the Sm^{3+} $N_{4,5}$ edges (purple line) resulting from a fit to the Sm_2O_3 data (see Fig. S2 in Appendix). The $N_{4,5}$ edge of Sm^{2+} (dark yellow line) was calculated using the same adjustable parameters as for Sm^{3+} (see below). The weighted sum (60% and 40%) of the simulated curves (dark cyan) describes the SmB_6 spectrum very well in the energy region between 120 and 135 eV. This is the region where the high multipole scattering dominates (see Fig. S3 of the Appendix and Ref. [66] for further explanation). In the region above ≈ 135 eV, where the spectrum

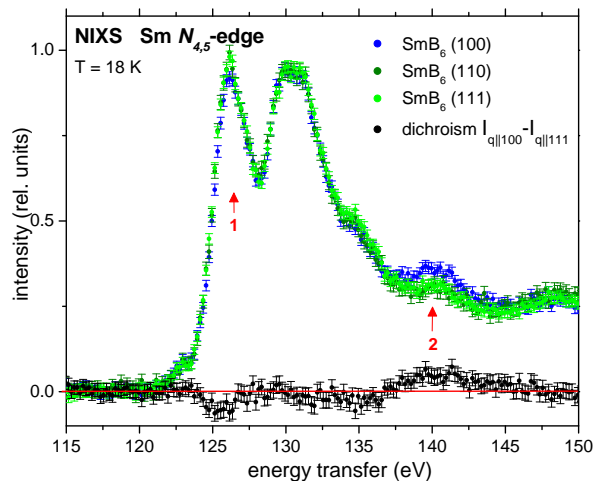


FIG. 4. (color online) SmB_6 NIXS data at 16 K for $\vec{q}||[100]$ (blue dots), $\vec{q}||[110]$ (dark green dots), and $\vec{q}||[111]$ (light green dots). The difference spectrum between the $\vec{q}||[100]$ and $\vec{q}||[111]$ directions is also displayed (black dots).

is given mostly by the dipole transitions (see Fig. S3 and Ref. [66]) the simulation produces spectral features that are too sharp with respect to the experiment because the interference with the continuum states is not included in the calculations. The high multipole excitations are more realistically reproduced since they are lower in energy and therefore further away from the continuum states and consequently more excitonic [76].

For the simulations of the $4d \rightarrow 4f$ transitions we used the full multiplet code *Quanty* which includes Coulomb and spin-orbit interactions [77]. A Gaussian and a Lorentzian broadening of 0.7 eV and 0.4 eV FWHM, respectively, account for the instrumental resolution and life-time effects. The atomic $4f-4f$ and $4d-4f$ Coulomb interactions were calculated using the Hartree-Fock scheme and a reduction of about 20% [78] has been applied to obtain the best agreement between the calculated and measured peak positions. This reduction accounts for configuration interaction processes not included in the Hartree-Fock scheme [79]. A momentum transfer of $|\vec{q}| = 9.8 \text{ \AA}^{-1}$ has been used for the simulations rather than the experimental value of $9.6 \pm 0.1 \text{ \AA}^{-1}$ in order to reproduce best the experimental peak intensity ratio of the two main features around 126 and 130 eV. This fine tuning optimizes the different multipole contributions to the scattering functions as shown in Fig. S3 of the Appendix and represents a minor adjustment of the calculated radial wave functions of the Sm^{3+} atomic wave function (see e.g. Ref. [59]).

Figure 4 shows the direction dependence of the Sm $N_{4,5}$ of SmB_6 . Although the effect is small, there are clear differences between the spectra in the energy regions marked with red arrows. At about 126 eV energy transfer

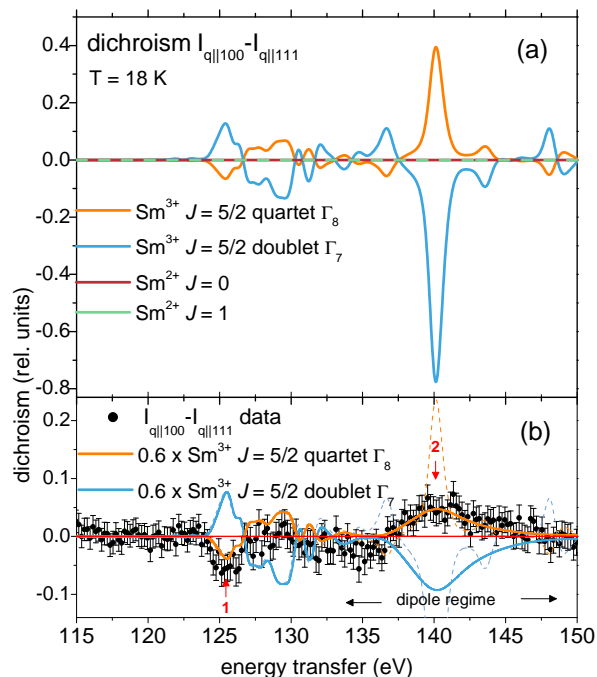


FIG. 5. (color online) (a) simulation of the $\vec{q}||[100]$ vs. $\vec{q}||[111]$ dichroic spectrum for the $J=0$ (brown) and $J=1$ (green) multiplet states of the Sm^{2+} configuration as well as for the Γ_8 quartet (orange) and Γ_7 doublet (light blue) of the $J=5/2$ Sm^{3+} configuration; (b) experimental dichroic spectrum (black dots) and simulated dichroic spectra for the Γ_8 quartet (orange) and Γ_7 doublet (light blue) scaled with the factor of 0.6 to account for the Sm^{3+} component of the ground state; dashed lines with energy independent broadening, solid lines with extra broadening in the dipole region (see text).

the scattering of the $\vec{q}||[110]$ (light green dots) and $\vec{q}||[111]$ (dark green dots) directions are both stronger than for the $\vec{q}||[100]$ (blue dots), and at about 140 eV it is opposite. To show these directional differences in a more transparent manner, we also present in Fig. 4 the difference spectrum between the $\vec{q}||[100]$ and $\vec{q}||[111]$ (black dots): this so-called dichroic spectrum has unambiguously a negative peak at 126 eV whereas it displays positive intensity in a broader region around 140 eV.

To interpret the observed direction dependence, it is important to know how each CEF state or multiplet component contributes to the dichroic signal. Therefore, $S(\vec{q}, \omega)$ has been calculated taking into account a cubic CEF for the Sm^{3+} f^5 ground state multiplet with $J=5/2$ assuming a Γ_8 quartet or a Γ_7 doublet ground state, and for the Sm^{2+} f^6 multiplets with $J=0$ or $J=1$ (see Fig. 1), [80]. The calculations were performed for the two directions $\vec{q}||[100]$ and $\vec{q}||[111]$ and in Fig. 5 (a) the resulting dichroic signals are plotted. The first important finding is that the Sm^{2+} configuration does not show any dichroism at all (see dark red and green lines at zero

dichroism) as we would expect for states with spherical charge densities (see Fig. 1). Hence, the observed direction dependence of the signal is solely due to the Sm^{3+} Hund's rule ground state. The second important finding is that the Γ_8 and Γ_7 CEF states exhibit different and opposite dichroism (see orange and light blue lines), consistent with their opposite anisotropy in the charge densities (see Fig. 1). These aspects facilitate the straight forward determination of the CEF ground state of Sm^{3+} in SmB_6 .

Figure 5 (b) shows the experimental dichroic spectrum (black dots) together with the calculated ones. The two possible CEF states of the $J=5/2$ configuration have now been scaled down to 60% to quantitatively account for the Sm^{3+} component in intermediate valent SmB_6 . We can clearly observe that in the regions of pronounced dichroism (see red arrows) the sign of the experimental dichroic signal is correctly explained by the Γ_8 quartet (orange line) but not at all by the Γ_7 doublet state (light blue line). In addition, the Γ_8 reproduces the experimental dichroism quantitatively in the high multipole region (see red arrow 1). The dichroism also fits quantitatively in the dipole region (see red arrow 2) when an extra broadening is applied (FWHM ≥ 4 eV beyond ≈ 135 eV energy transfer) to mimic the interference with continuum states. The dashed lines correspond to the dipole calculation without the extra broadening. These results unambiguously establish that the CEF ground state of the $\text{Sm} f^5$ component in SmB_6 is the Γ_8 quartet.

We would like to point out that the down scaling to 60% of the $\text{Sm} f^5$ component gives a good quantitative agreement in the magnitude of the dichroic signal. This provides confidence that the NIXS method is indeed reliable since this 60% number is fully consistent with the existing valence determination in the literature [40–46] as well as with the above analysis of the total $N_{4,5}$ NIXS spectra. We also would like to note that possible errors in the alignment of the Sm^{2+} NIXS signal with respect to that of the Sm^{3+} do not affect the dichroic signal and hence the analysis of the CEF ground state since the Sm^{2+} is silent in terms of directional dependence.

Our finding of the Γ_8 quartet forming the ground state supports very much the results of spin resolved APRES [22]. Xu *et al.* find spin polarized surface states, fulfilling time reversal as well as crystal symmetry, that have spins locked to the crystal momenta k such that at opposite momenta the surface states have opposite spins. The anticlockwise spin texture is in agreement with spin expectation values that are calculated by Baruselli and Vojta for a Γ_8 ground state [48, 50]. Note, for a Γ_7 the spin directions should be reversed.

To summarize, we have utilized the high multipole contributions in the core-level non-resonant inelastic x-ray scattering process to determine the symmetry of the Sm crystal field ground state $4f$ wave function in SmB_6 . We have found a clear directional dependence of the spectra

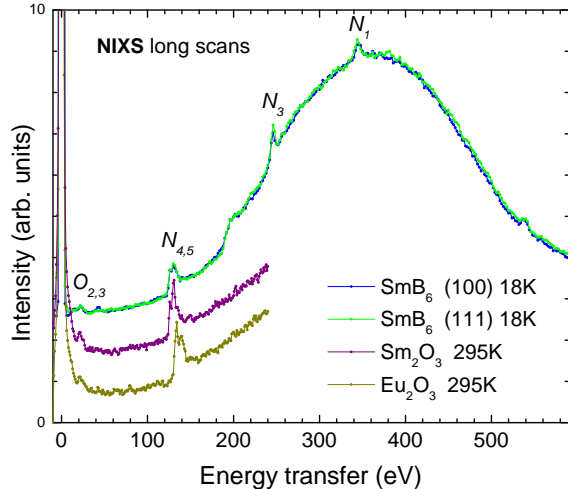


FIG. S1 (color online) Energy scans of SmB_6 for $\vec{q} \parallel [100]$ and $\vec{q} \parallel [111]$, Sm_2O_3 and Eu_2O_3 measured at $|\vec{q}| = (9.6 \pm 0.1) \text{ \AA}^{-1}$ and with a constant final energy of 9690 eV over a wide energy ranges, for SmB_6 with 0.5 eV energy steps, for Sm_2O_3 and Eu_2O_3 with 0.2 eV; shifted for clarity.

that allows for the unambiguous identification of the Γ_8 quartet state of the Sm $f^5 J=5/2$ configuration as the state which governs the topological properties of SmB_6 .

ACKNOWLEDGMENT

We thank C. Becker and T. Mende from MPI-CPfS, and F.-U. Dill, S. Mayer, C.J. Sahle and M. Harder from PETRA III at DESY (a member of the Helmholtz Association - HGF) for their skillful technical support. K.C., M.S., A.S., and D.K. benefited from the financial support of the Deutsche Forschungsgemeinschaft under projects SE 1441 and SPP 1666.

APPENDIX

Fig. S1 shows non-resonant inelastic x-ray scattering (NIXS) spectra of SmB_6 (blue and green line) measured over a large energy interval and of the two reference compounds Sm_2O_3 and Eu_2O_3 (purple and dark yellow) measured up to 250 eV energy transfer. The strongest signal is the elastic line, followed by shallow Sm/Eu core resonances (O-edges) and the Sm/Eu $N_{4,5}$ -edges at about 130 and 135 eV sitting on top of the rising Compton background. The spectra are offset on the y-axis by 1 unit after scaling to the Compton background.

Fig. S2 shows the fit (red line) of the Sm_2O_3 NIXS data (purple dots) at the Sm $N_{4,5}$ -edge using the full multiplet code *Quanty* [77]. In the multipole region the agreement between calculation and data is good, in the dipole region the simulation yields unrealistically sharp features since

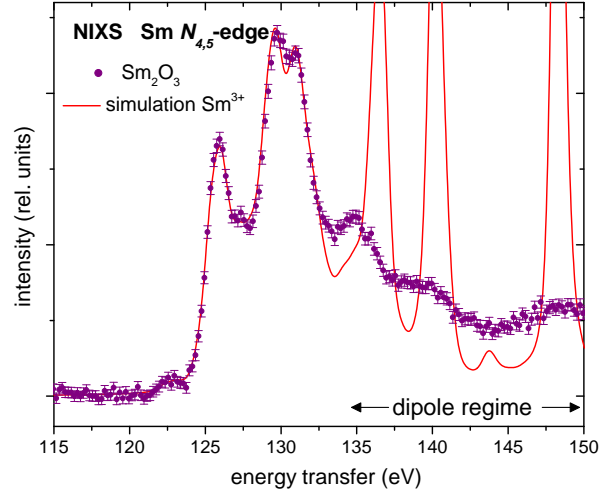


FIG. S2 (color online) N -edge data of Sm_2O_3 (purple dots) measured with $|\vec{q}| = (9.6 \pm 0.1) \text{ \AA}^{-1}$ for a constant final energy of 9690 eV and simulation (red line).

interference with continuum states are not included in the calculation.

In scattering experiments at large momentum transfers $|\vec{q}|$ the scattering function $S(\vec{q}, \omega)$ contains higher than dipole terms. Fig. S3 (a) shows the radial part of $S(\vec{q}, \omega)$ for dipole ($k=1$ red line) and higher orders ($k=3$, and 5; green and blue lines). Already at $|\vec{q}| \cong 10 \text{ \AA}^{-1}$ the higher order terms amount to about 50% of the total scattering intensity. Note, 10 \AA^{-1} is accessible in a hard x-ray NIXS experiment. The excitations due to $k=3$ and 5 appear lower in energy than the dipole excitations (see fig. S3 (b)). Not only the sensitivity of beyond dipole scattering to higher than two-fold symmetries is an advantage, in addition these beyond dipole excitations are more excitonic (see e.g. in Ref. [66, 69]). The method is bulk sensitive and can be modeled quantitatively (see e.g. Ref. [59, 60, 62, 75]).

-
- [1] A. Menth, E. Buehler, and T. H. Geballe, Phys. Rev. Lett. **22**, 295 (1969).
 - [2] R. L. Cohen, M. Eibschütz, and K. W. West, Phys. Rev. Lett. **24**, 383 (1970).
 - [3] J. W. Allen, B. Batlogg, and P. Wachter, Phys. Rev. B **20**, 4807 (1979).
 - [4] B. Gorshunov, N. Sluchanko, A. Volkov, M. Dressel, G. Knebel, A. Loidl, and S. Kunii, Phys. Rev. B **59**, 1808 (1999).
 - [5] P. S. Riseborough, Adv. Phys. **49**, 257 (2000).
 - [6] M. Dzero, K. Sun, V. Galitski, and P. Coleman, Phys. Rev. Lett. **104**, 106408 (2010).
 - [7] T. Takimoto, J. Phys. Soc. Jpn. **80**, 123710 (2011).
 - [8] M. Dzero, K. Sun, P. Coleman, and V. Galitski, Phys. Rev. B **85**, 045130 (2012).

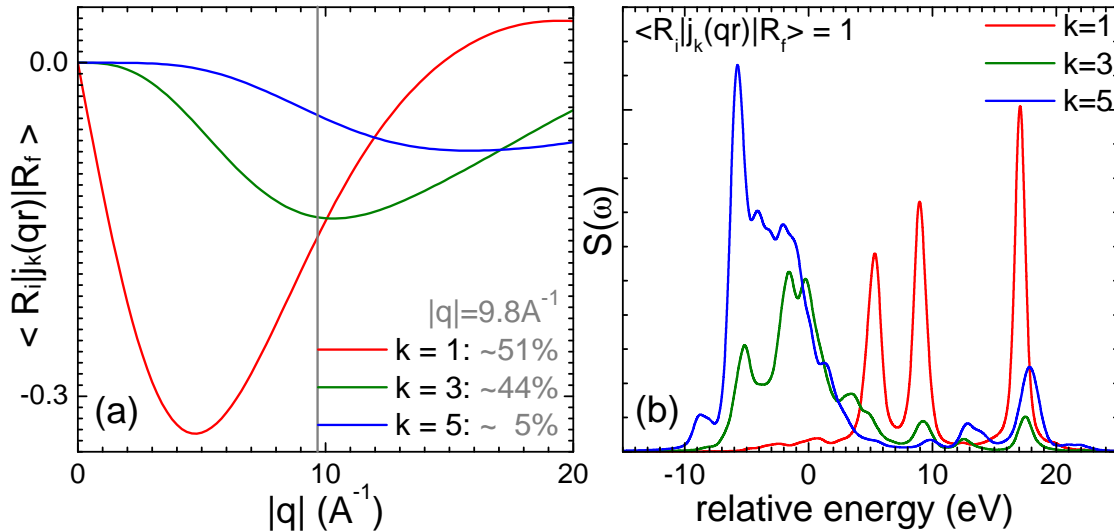


FIG. S3 (color online) Momentum $|\vec{q}|$ dependence (left) and energy dependence (right) of the scattering function $S(\vec{q}, \omega)$ at the Sm $N_{4,5}$ -edge for dipole ($k=1$), octupole ($k=3$), and dotriacontapole ($k=5$) scattering orders. The grey vertical line marks the $|\vec{q}|$ -range of the experiment.

- [9] F. Lu, J. Z. Zhao, H. Weng, Z. Fang, and X. Dai, Phys. Rev. Lett. **110**, 096401 (2013).
- [10] M. Dzero and V. Galitski, J. Exp. Theo. Phys. **117**, 499 (2013).
- [11] V. Alexandrov, M. Dzero, and P. Coleman, Phys. Rev. Lett. **111**, 226403 (2013).
- [12] A. Vishwanath and T. Senthil, Phys. Rev. X **3**, 011016 (2013).
- [13] P. Bonderson, C. Nayak, and X.-L. Qi, Journal of Statistical Mechanics: Theory and Experiment **2013**, P09016 (2013).
- [14] C. Wang, A. C. Potter, and T. Senthil, Phys. Rev. B **88**, 115137 (2013).
- [15] L. Fidkowski, X. Chen, and A. Vishwanath, Phys. Rev. X **3**, 041016 (2013).
- [16] N. Xu, X. Shi, P. K. Biswas, C. E. Matt, R. S. Dhaka, Y. Huang, N. C. Plumb, M. Radović, J. H. Dil, E. Pomjakushina, K. Conder, A. Amato, Z. Salman, D. M. Paul, J. Mesot, H. Ding, and M. Shi, Phys. Rev. B **88**, 121102 (2013).
- [17] Z.-H. Zhu, A. Nicolaou, G. Levy, N. P. Butch, P. Syers, X. F. Wang, J. Paglione, G. A. Sawatzky, I. S. Elfimov, and A. Damascelli, Phys. Rev. Lett. **111**, 216402 (2013).
- [18] M. Neupane, N. Alidoust, S.-Y. Xu, T. Kondo, Y. Ishida, D. J. Kim, C. Liu, I. Belopolski, Y. J. Jo, T.-R. Chang, H.-T. Jeng, T. Durakiewicz, L. Balicas, H. Lin, A. Bansil, S. Shin, Z. Fisk, and M. Hasan, Nat. Commun. **4**, 2991 (2013).
- [19] J. Jiang, S. Li, T. Zhang, Z. Sun, F. Chen, Z. Ye, M. Xu, Q. Ge, S. Tan, X. Niu, M. Xia, B. Xie, Y. Li, X. Chen, H. Wen, and D. Feng, Nature Comm. **4**, 3010 (2013).
- [20] J. Denlinger, J. W. Allen, J.-S. Kang, K. Sund, J.-W. Kim, J. H. Shim, B. I. Min, D.-J. Kim, and Z. Fisk, arXiv:1312.6637 (2013).
- [21] J. D. Denlinger, J. W. Allen, J.-S. Kang, K. Sun, B.-I. Min, D.-J. Kim, and Z. Fisk, JPS Conf. Proc. **3**, 017038 (2014).
- [22] N. Xu, P. K. Biswas, J. H. Dil, R. S. Dhaka, G. Landolt, S. Muff, C. E. Matt, X. Shi, N. C. Plumb, M. Radovic, E. Pomjakushina, K. Conder, A. Amato, S. V. Borisenko, R. Yu, H.-M. Weng, Z. Fang, X. Dai, J. Mesot, H. Ding, and M. Shi, Nat. Commun. **5**, 4566 (2014).
- [23] N. Xu, C. E. Matt, E. Pomjakushina, X. Shi, R. S. Dhaka, N. C. Plumb, M. Radović, P. K. Biswas, D. Evtushinsky, V. Zabolotnyy, J. H. Dil, K. Conder, J. Mesot, H. Ding, and M. Shi, Phys. Rev. B **90**, 085148 (2014).
- [24] P. Hlawenka, K. Siemensmeyer, E. Weschke, A. Varykhalov, J. Sanchez-Barriga, N. Y. Shitsevalova, A. V. Dukhnenko, V. B. Filipov, S. Gabni, S. Flachbart, O. Rader, and E. D. L. Rienks, arXiv:1312.6637 (2015).
- [25] M. M. Yee, Y. He, A. Soumyanarayanan, D. J. Kim, Z. Fisk, and J. E. Hoffman, arXiv:1308.1085 (2013).
- [26] S. Rössler, T.-H. Jang, D.-J. Kim, T. L.H., Z. Fisk, and S. Steglich, F. Wirth, Proc. Nat. Acad. Science. U.S.A. **111**, 4798 (2014).
- [27] W. Ruan, C. Ye, M. Guo, F. Chen, X. Chen, G.-M. Zhang, and Y. Wang, Phys. Rev. Lett. **112**, 136401 (2014).
- [28] S. Rössler, L. Jiao, D. J. Kim, S. Seiro, K. Rasim, F. Steglich, L. H. Tjeng, Z. Fisk, and S. Wirth, Philosophical Magazine **96**, 3262 (2016).
- [29] L. Jiao, S. Rössler, D. J. Kim, L. H. Tjeng, Z. Fisk, F. Steglich, and S. Wirth, Nature Commun. **7**, 13762 (2016).
- [30] M. C. Hatnean, M. R. Lees, D. M. K. Paul, and G. a. Balakrishnan, Scientific Reports , 3403 (2013).
- [31] X. Zhang, N. P. Butch, P. Syers, S. Ziemak, R. L. Greene, and J. Paglione, Phys. Rev. X **3**, 011011 (2013).
- [32] D. J. Kim, S. Thomas, T. Grant, J. Botimer, Z. Fisk, and J. Xia, Scientific Reports **3**, 3150 (2013).

- [33] S. Wolgast, C. Kurdak, K. Sun, J. W. Allen, D.-J. Kim, and Z. Fisk, *Phys. Rev. B* **88**, 180405 (2013).
- [34] D. J. Kim, J. Xia, and Z. Fisk, *Nat. Mater.* **13**, 466 (2014).
- [35] S. Wolgast, Y. S. Eo, T. Öztürk, G. Li, Z. Xiang, C. Tinsman, T. Asaba, B. Lawson, F. Yu, J. W. Allen, K. Sun, L. Li, C. Kurdak, D.-J. Kim, and Z. Fisk, *Phys. Rev. B* **92**, 115110 (2015).
- [36] S. Thomas, D. J. Kim, S. B. Chung, T. Grant, Z. Fisk, and J. Xia, *Phys. Rev. B* **94**, 205114 (2016).
- [37] Y. Nakajima, P. Syers, X. Wang, R. Wang, and J. Paglione, *Nat. Phys.* **12**, 213 (2016).
- [38] M. Dzero, J. Xia, V. Galitski, and P. Coleman, *Annual Rev. Con. Mat Phys.* **7** (2016).
- [39] J. W. Allen, *Philosophical Magazine* **96**, 3227 (2016).
- [40] J. W. Allen, L. I. Johansson, I. Lindau, and S. B. Hagstrom, *Phys. Rev. B* **21**, 1335 (1980).
- [41] J. M. Tarascon, Y. Ishikawa, B. Chevalier, J. Etourneau, P. Hagemuller, and K. M., *J. Physique* **41**, 1141 (1980).
- [42] M. Mizumaki, S. Tsutsui, and I. F., *J. Phys.: Conf. Ser.* **176**, 012034 (2009).
- [43] H. Hayashi, N. Kanai, N. Kawamura, M. Mizumaki, K. Imura, N. K. Sato, H. S. Suzuki, and F. Iga, *J. Anal. At. Spectrom.* **28**, 378 (2013).
- [44] P. Lutz, M. Thees, T. R. Peixoto, B. Y. Kang, B. K. Cho, C. H. Min, and F. Reinert, *Philosophical Magazine* **96**, 3307 (2016).
- [45] N. P. Butch, J. Paglione, P. Chow, Y. Xiao, C. A. Marianetti, C. H. Booth, and J. R. Jeffries, *Phys. Rev. Lett.* **116**, 156401 (2016).
- [46] Y. Utsumi, D. Kasinathan, K.-T. Ko, S. Agrestini, M. Haverkort, S. Wirth, Y.-H. Wu, K.-D. Tsuei, D.-J. Kim, Z. Fisk, P. Thalmeier, and L. Tjeng, *arXiv:1705.03459* (2017).
- [47] K. Lea, M. Leask, and W. Wolf, *Journal of Physics and Chemistry of Solids* **23**, 1381 (1962).
- [48] P. P. Baruselli and M. Vojta, *Phys. Rev. Lett.* **115**, 156404 (2015).
- [49] M. Legner, A. Rüegg, and M. Sigrist, *Phys. Rev. Lett.* **115**, 156405 (2015).
- [50] P. P. Baruselli and M. Vojta, *Phys. Rev. B* **93**, 195117 (2016).
- [51] P. Alekseev, V. Lazukov, R. Osborn, B. Rainford, I. Sadikov, E. Konovalova, and Y. Paderno, *Euro. Phys. Lett.* **23**, 347 (1993).
- [52] P. A. Alekseev, J. M. Mignot, J. Rossat-Mignod, V. N. Lazukov, I. P. Sadikov, E. S. Konovalova, and Y. B. Paderno, *Journal of Physics: Condensed Matter* **7**, 289 (1995).
- [53] W. T. Fuhrman, J. Leiner, P. Nikolić, G. E. Granroth, M. B. Stone, M. D. Lumsden, L. DeBeer-Schmitt, P. A. Alekseev, J.-M. Mignot, S. M. Koohpayeh, P. Cottingham, W. A. Phelan, L. Schoop, T. M. McQueen, and C. Broholm, *Phys. Rev. Lett.* **114**, 036401 (2015).
- [54] P. Nyhus, S. L. Cooper, Z. Fisk, and J. Sarrao, *Phys. Rev. B* **52**, R14308 (1995).
- [55] P. Nyhus, S. L. Cooper, Z. Fisk, and J. Sarrao, *Phys. Rev. B* **55**, 12488 (1997).
- [56] B. Frick and M. Loewenhaupt, *Zeitschrift für Physik B Condensed Matter* **63**, 213 (1986).
- [57] E. Zirngiebl, B. Hillebrands, S. Blumenröder, G. Güntherodt, M. Loewenhaupt, J. M. Carpenter, K. Winzer, and Z. Fisk, *Phys. Rev. B* **30**, 4052 (1984).
- [58] M. Loewenhaupt and M. Prager, *Zeitschrift für Physik B Condensed Matter* **62**, 195 (1986).
- [59] T. Willers, F. Strigari, N. Hiraoka, Y. Q. Cai, M. W. Haverkort, K.-D. Tsuei, Y. F. Liao, S. Seiro, C. Geibel, F. Steglich, L. H. Tjeng, and A. Severing, *Phys. Rev. Lett.* **109**, 046401 (2012).
- [60] J.-P. Rueff, J. M. Ablett, F. Strigari, M. Deppe, M. W. Haverkort, L. H. Tjeng, and A. Severing, *Phys. Rev. B* **91**, 201108 (2015).
- [61] M. Sundermann, F. Strigari, T. Willers, H. Winkler, A. Prokofiev, J. M. Ablett, J.-P. Rueff, D. Schmitz, E. Weschke, M. M. Sala, A. Al-Zein, A. Tanaka, M. W. Haverkort, D. Kasinathan, L. H. Tjeng, S. Paschen, and A. Severing, *Scientific Report* **5**, 17937 (2015).
- [62] M. Sundermann, M. W. Haverkort, S. Agrestini, A. Al-Zein, M. M. Sala, Y. Huang, M. Golden, A. de Visser, P. Thalmeier, L. H. Tjeng, and A. Severing, *Proc. Nat. Acad. Science. U.S.A.* **113**, 13989 (2016).
- [63] J. A. Soininen, A. L. Ankudinov, and J. J. Rehr, *Phys. Rev. B* **72**, 045136 (2005).
- [64] B. C. Larson, W. Ku, J. Z. Tischler, C.-C. Lee, O. D. Restrepo, A. G. Eguiluz, P. Zschack, and K. D. Finkelstein, *Phys. Rev. Lett.* **99**, 026401 (2007).
- [65] M. W. Haverkort, A. Tanaka, L. H. Tjeng, and G. A. Sawatzky, *Phys. Rev. Lett.* **99**, 257401 (2007).
- [66] R. A. Gordon, G. T. Seidler, T. T. Fister, M. W. Haverkort, G. A. Sawatzky, A. Tanaka, and T. K. Sham, *EPL (Europhysics Letters)* **81**, 26004 (2008).
- [67] R. Gordon, M. Haverkort, S. Sen Gupta, and S. G.A., *J. Phys. Conf. Ser.* **190**, 012047 (2009).
- [68] J. A. Bradley, S. Sen Gupta, G. T. Seidler, K. T. Moore, M. W. Haverkort, G. A. Sawatzky, S. D. Conradson, D. L. Clark, S. A. Kozimor, and K. S. Boland, *Phys. Rev. B* **81**, 193104 (2010).
- [69] R. Caciuffo, G. van der Laan, L. Simonelli, T. Vitova, C. Mazzoli, M. A. Denecke, and G. H. Lander, *Phys. Rev. B* **81**, 195104 (2010).
- [70] J.-P. Rueff and A. Shukla, *Rev. Mod. Phys.* **82**, 847 (2010).
- [71] N. Hiraoka, M. Suzuki, K. D. Tsuei, Y. Q. Cai, M. W. Haverkort, C. C. Lee, and K. Ku, *EPL* **96** (2011).
- [72] S. Sen Gupta, J. A. Bradley, M. W. Haverkort, G. T. Seidler, A. Tanaka, and G. A. Sawatzky, *Phys. Rev. B* **84**, 075134 (2011).
- [73] J. A. Bradley, K. T. Moore, G. van der Laan, J. P. Bradley, and R. A. Gordon, *Phys. Rev. B* **84**, 205105 (2011).
- [74] G. van der Laan, *Phys. Rev. Lett.* **108**, 077401 (2012).
- [75] M. Sundermann, K. Chen, H. Yava, H. Lee, Z. Fisk, M. W. Haverkort, L. H. Tjeng, and A. Severing, *EPL* **117**, 17003 (2017).
- [76] S. Sen Gupta, J. A. Bradley, M. W. Haverkort, G. T. Seidler, A. Tanaka, and G. A. Sawatzky, *Phys. Rev. B* **84**, 075134 (2011).
- [77] M. W. Haverkort, *J. Phys.: Conf. Ser.* **712**, 012001 (2016).
- [78] The $4d-4f$ Slater integral G1 has been reduced another 15% to about 68%.
- [79] A. Tanaka and T. Jo, *J Phys. Soc. Jpn.* **63**, 2788 (1994).
- [80] The excited $J = 7/2$ multiplet is not considered because it will not contribute since it is too high in energy.